Composites Part B 259 (2023) 110728

Contents lists available at ScienceDirect

Composites Part B

journal homepage: www.elsevier.com/locate/compositesb

Fatigue-resistant, single-phase stretchable materials via crack bridging

Dani Liu [a], Shuofei Sun [b], Gening Dong [b], Feifei Long [b], Mingkun Wang [a,b,*]

[a] School of Aeronautic Science and Engineering, Beihang University, Beijing, 100191, China
[b] Meinig School of Biomedical Engineering, Cornell University, Ithaca, NY, 14853, USA

ARTICLE INFO

Handling Editor: Dr Hao Wang

Keywords:
Polymer fibers
Polymer-matrix composites
Thermosetting resin
Fatigue
Fracture toughness

ABSTRACT

Stretchable materials such as elastomers and hydrogels are vulnerable to the growth of a crack under repeated cycles of stretch. This is because in single-network/phase materials, the crack can easily propagate by fracturing a single layer of polymer chains. Therefore, to improve the fatigue resistance of stretchable materials, current methods focus on blocking the crack front by another intrinsically high-energy phase. Such high-energy phases, however, are often limited to specific polymers or compromise other properties, limiting its extension to other fields. Single material approaches have been used in structural materials but considered inapplicable to soft materials. Here we challenge this acknowledgement by demonstrating the crack bridging effect in micro-patterned elastomers. Instead of resisting in front of crack tips, micropatterns shield polymer chains by bridging behind the crack front. To utilize the bridging effect, we create composites with one material. They are structurally one piece of material but have molecularly separated fibers and matrices due to different curing mechanisms of components. Single-phase composites of polydimethylsiloxane (PDMS) made by this strategy have a fatigue threshold three times higher than that of PDMS-hydrogel composites designed based on the classic high-energy strategy. This crack bridging strategy does not rely on the inter- and intra-polymer interactions provided by specific materials, and thus have a general usefulness.

1. Introduction

Stretchable materials have wide industrial applications in sealing and dampening, and help launch emerging fields such as soft robots [1–4], bioelectronics [5–8], and tissue replacements [9–11]. A well-known problem of those materials is the fast crack propagation under cyclic loads. This can cause significant failures, from spacecraft to appliances, and is a drag on commercialization of emerging applications. Single-phase materials are especially unwelcome in load-bearing applications, as cracks can easily propagate by fracturing a single layer of polymer chains [12–15].

The fatigue cracks can be pinned by intrinsically high-energy phase, including nanocrystalline domains [16–18], nanofibers [19,20], separated microphase [21,22], and macro-fibers [23,24]. This has become a widely-acknowledged design principle for fatigue resistant soft materials [25]. For example, the combination of freeze casting and salting out created a hierarchically anisotropic polyvinyl alcohol hydrogel (HA-PVA) [26]. It consists of micrometer-scale fibers, which in turn comprise interconnected nanocrystalline fibrils. Such PVA hydrogels have by far the highest fatigue threshold among soft materials, well above 10000 J/m^2. However, this method is generally limited to PVA. By contrast, although biomaterials such as gelatin made by the same freeze casting and salting out also had hierarchically anisotropic structure, they had a fatigue threshold only on the order of 10 J/m^2. This is largely because gelatin forms aggregations instead of nanocrystals [27], and those aggregations dissociate under repeated loading. Natural rubber, on the other hand, despite its stretch-induced crystalline domains, has a fatigue threshold only around 50 J/m^2. Another example of the high-energy phase strategy is the composites of polydimethylsiloxane (PDMS) fibers and polyacrylamide (PAAm) hydrogel matrices. The Young's modulus of PDMS was above 2 MPa while the PAAm was much softer with a modulus of around 100 KPa. The millimeter-scale PDMS fibers and PAAm matrices were chemically crosslinked, but due to their huge stiffness contrast, stress was distributed along fibers instead of localized on the crack tip. This gives PDMS-hydrogel composite a fatigue threshold of 1250 J/m^2 [24], but the weak hydrogel matrices significantly reduce the strength of resultant composites.

Crack bridging is an important toughening mechanism for structural composites [28,29]. However, it is generally considered inapplicable to soft materials. Because when fibers and matrices were integrated, the

* Corresponding author. School of Aeronautic Science and Engineering, Beihang University, Beijing, 100191, China.
E-mail address: mw786@cornell.edu (M. Wang).

https://doi.org/10.1016/j.compositesb.2023.110728
Received 1 December 2022; Received in revised form 23 March 2023; Accepted 4 April 2023
Available online 13 April 2023

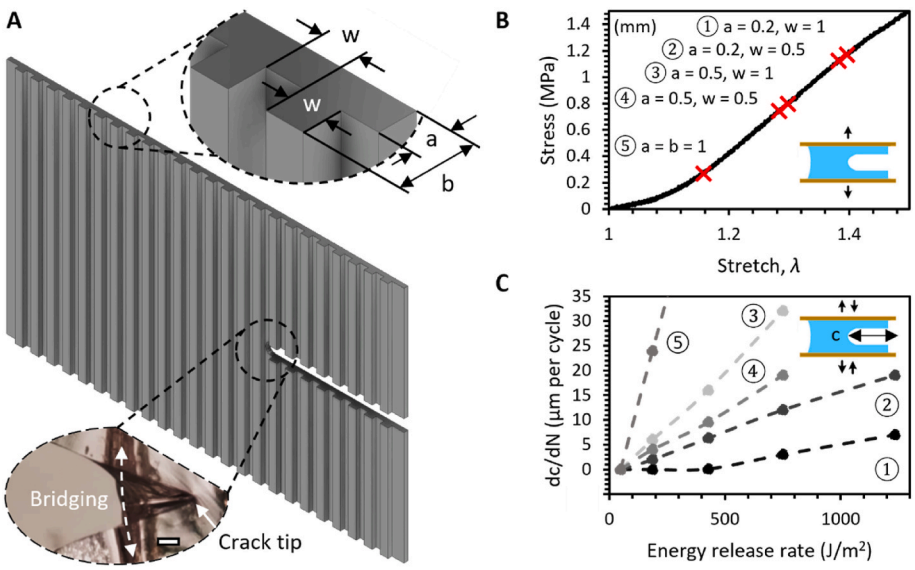

Fig. 1. Micropatterned PDMS. (**A**) Crack bridging improved fracture toughness and fatigue threshold of micropatterned PDMS. (**B**) The stress-stretch curve of intact PDMS, red crosses are the points when crack propagated in the precut micropatterned and homogeneous PDMS. Fracture toughness is the area under the curve up to fracture point. (**C**) Crack growth in micropatterned and homogeneous PDMS per cycle under different energy release rates. Fatigue threshold is the maximum energy release rate at $dc/dN = 0$. Scale bar = 100 μm. (For interpretation of the references to colour in this figure legend, the reader is referred to the Web version of this article.)

soft composites were as fragile as homogenous materials, while when fibers and matrices were completely separated, cracks propagated through the matrices regardless of fibers [23]. Here we first demonstrated the effect of crack bridging in stretch materials. The bridging effect was activated simply by micropatterns, when cracks propagated from thin features into thick features. We next implemented this effect by a strategy autologous to ceramic composites. The success of ceramic composites comes from a sophisticated design of fiber-matrix interface [30]. Here we achieved the "goldilocks" fiber-matrix interface by crosslinking the same materials with different mechanisms. As a demonstration, we created composites of PDMS microfibers and matrices with the same crosslinking ratio. Fibers were fabricated by a "fry-spinning" technique and crosslinked by radical curing, while matrices crosslinked with addition curing by a platinum catalyzer. The different curing mechanisms led to a weak molecular link but structural integration between fibers and matrices. The single-phase PDMS composites had a fatigue threshold of 4500 J/m^2, three times higher than the PDMS-hydrogel composites, which is designed based on the classic principle of high-energy phase. More importantly, the single-phase PDMS composites maintain the strength and mechanical robustness of bulk PDMS.

2. Material and methods

2.1. Materials

Sylgard 184 (Dow Corning, Midland, MI) is a two-part kit consisting of an elastomeric prepolymer (Part A) and a crosslinker (Part B) and was mixed at the standard 10:1 prepolymer to crosslinker ratio, unless explicitly stated otherwise. The platinum catalyst utilized in this work was an Ashby-Karstedt catalyst, a mid-temperature platinum-cyclovinylmethylsiloxane complex containing 2 wt% platinum in cyclomethylvinylsiloxanes was supplied by Gelest (SIP 6832.2).

2.2. Fabrication of micropatterned PDMS

Micropatterned PVA molds were 3D printed by a commercial printer with nozzle size of 0.2 mm and resolution of 0.12 mm. Liquid PDMS precursor, with a base to curing agent ratio of 10:1, was cast onto the molds. It was vacuumed for 30 min before being cured in an oven at 65 °C for 12 h. The crosslinked PDMS was retrieved by dissolving PVA in water.

2.3. Fry spinning of PDMS fibers

Liquid PDMS precursor was prepared by mixing base and curing agent at a ratio of 10:1. It was degassed by vacuum for 30 min to remove bubbles, and then transferred to a 10 ml syringe. The syringe stood for another 30 min to let small bubbles accumulate. After squeezing out bubbles, the syringe was fixed on a syringe pump and secured 200 mm above a hot plate. An oil bath was heated to 230 °C on the hot plate and the liquid precursor was extruded through flush needles into the oil bath. The syringe pump provided a flow rate of 30 ml/min for 10 ml syringe without needles, 6 ml/min for 18-gauge needles, and 0.6 ml/min for 24-gauge needles. The extruded threads of the precursor were cured immediately into fibers and collected by a customized stirring frame. The fiber diameter is controlled collectively by the viscosity of liquid precursor and the inner diameter of syringe needles. According to the manufacturer's instruction, the viscosity of the liquid precursor doubles every 3 h, so the vacuum and waiting times would influence the as-spun diameter. After retrieving from oil, the fibers were washed in isopropanol alcohol three times.

2.4. Fabrication of single-phase PDMS composites

PDMS microfibers were arranged in a Teflon mold with a thickness of 0.8 mm. Liquid PDMS precursor, with a base to curing agent ratio of 10:1, was uniformly dropped onto fibers. The weight to volume ratio of fibers to precursors was tuned around 2:1. The liquid precursor was vacuumed again, then covered by an acrylic sheet and placed in the oven at 65 °C for 12 h to crosslink.

2.5. Measurement of fracture toughness

The fracture toughness was measured by pure shear tests with a Mark-10 F105 and a 250 N load sensor. Each group had two identical samples (width: $L = 50$ mm, height between two grippers: $h = 10$ mm, thickness: $t = 1$ mm). They were loaded in uniaxial tension at a strain rate of 1%/s until fracture. The notched sample with a 15 mm pre-cut crack was used to find the critical stretch λ_c, while the unnotched sample was used to measure the stress-stretch curve. The area under stress-stretch curves up to the critical stretch is the elastic energy density $W(\lambda)$. The fracture toughness is given by $\Gamma = W(\lambda_c)h$.

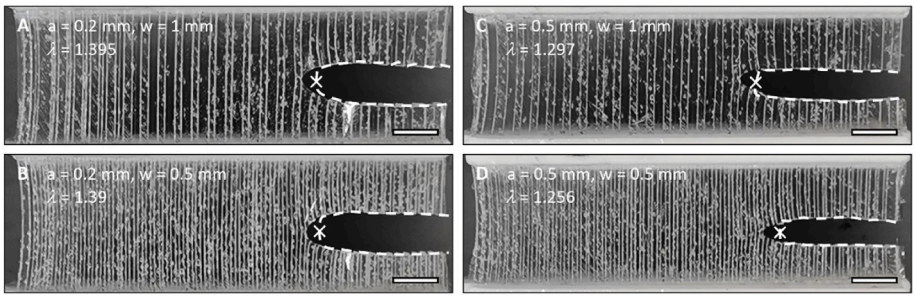

Fig. 2. Fracture toughness measurements for (**A**) thin and wide features, (**B**) thin and small features, (**C**) thick and large features, and (**D**) thick and small features. The arrows delineate the distances of crack propagation. Scale bar = 5 mm.

2.6. Measurement of fatigue threshold

The fracture-fatigue threshold was also measured by pure shear tests. Samples in each group were loaded in cyclic fatigue to the same strain at a frequency of 0.5 Hz for 30000 cycles. The notched sample was used to record the crack growth by each loading cycle dc/dN, while the unnotched sample was used to measure the stress-strain curve. The energy release rate $G = W(\lambda_m)h$. The fracture-fatigue threshold is the maximum G for $dc/dN = 0$.

3. Results and discussion

3.1. Crack bridging in stretchable materials

To demonstrate the applicability of crack bridging in stretchable materials, we fabricated a micropatterned PDMS (Fig. 1A). The base to curing agent ratio was 10:1. The thickness of grooves is denoted as a, while the overall thickness of the material is b. When cracks propagated from grooves to ridges, the intact part of ridges bridged the crack behind the tip to compete with the "opening" ahead of the crack tip. A larger ratio of a/b should in theory give a thicker bridging zone, and a wider w should give a longer bridging zone. To visualize the crack bridging effect, we prepared five samples with: 1. thin and wide ($a = 0.2$, $w = 1$); 2. thin and small ($a = 0.2$, $w = 0.5$); 3. thick and wide ($a = 0.5$, $w = 1$); 4. thick and small features ($a = 0.5$, $w = 0.5$); and 5. homogeneous PDMS ($a = b = 1$) as the control.

To measure the fracture toughness, we created precut cracks on samples and loaded them with uniaxial tension until fracture. The fracture toughness is given by $\Gamma = W(\lambda_c)h_0$, where λ_c is the critical stretch – the points when samples fracture, $W(\lambda_c)$ is the elastic energy density – the area under the stress-stretch curve of intact PDMS up to fracture, and h_0 is samples' original height. The fracture points of grooved PDMS went up along the stress-strain curve with decreasing a (Fig. 1B). The fracture points with the same a stayed closely, suggesting w had a little impact on fracture toughness. All those points were much higher than the fracture point of non-patterned PDMS. The grooved PDMS with $a = 0.2$ mm had a λ_c close to 1.4 (Fig. 2A), regardless of w (Fig. 2B). The λ_c of grooved PDMS with $a = 0.5$ mm approached to 1.3 when $w = 1$ mm (Fig. 2C) but was smaller when $w = 0.5$ mm (Fig. 2D). As $\Gamma \sim \lambda_c$.

These results supported that the fracture toughness was mainly determined by the thickness of thin patterns a. This is because under a single cycle of loading, the crack must fracture a whole pattern to propagate. When it advanced from thin patterns into thick patterns, the higher area ratios of thick patterns over thin patterns, the higher energy density required to fracture those thick patterns.

To measure the fatigue threshold, we loaded the samples in cyclic fatigue to constant stretches. The threshold is the maximum energy release rate G when the speed of crack propagation, $dc/dN = 0$, where c is the crack length and N is the number of loading cycles. The energy release rate is given by $G = W(\lambda_m)h_0$. The results showed that grooved PDMS with $a = 0.2$ mm and $w = 1$ mm, had a remarkably higher threshold than other groups (Fig. 1C). When w was fixed, small a led to a higher fatigue threshold.

The speed of crack growth can help visualize the influence of crack bridging on fatigue threshold. Under cyclic fatigue loads to $\lambda = 1.2$, the crack was still locked in the first ridge of grooved PDMS with $a = 0.2$ mm and $w = 1$ mm, even after 10,000 cycles (Fig. 3A). By contrast, the crack expanded more than 15% of sample length during just 1000 cycles in grooved PDMS with $a = 0.2$ mm and $w = 0.5$ mm (Fig. 3B), more than

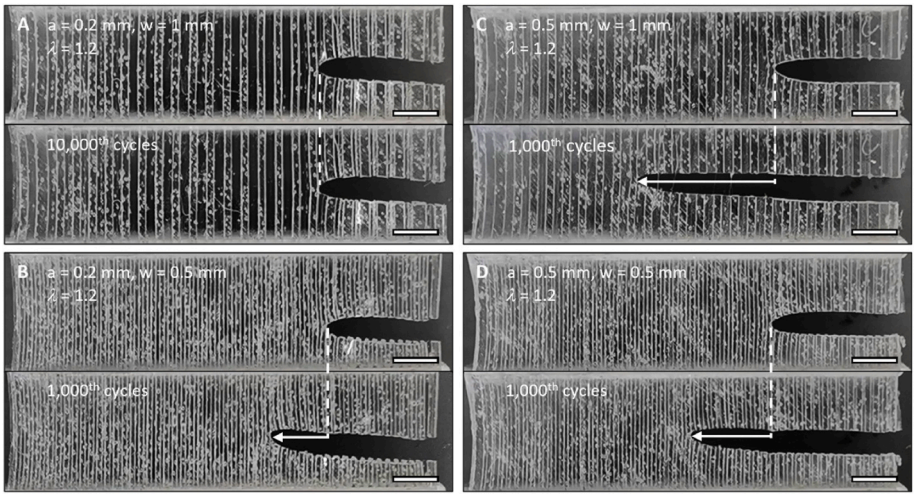

Fig. 3. Crack bridging slowed down crack growth. Speed of crack growth in micropatterned PDMS with (**A**) thin and wide features, (**B**) thin and small features, (**C**) thick and large features, and (**D**) thick and small features. The arrows delineate the distances of crack propagation. Scale bar = 5 mm.

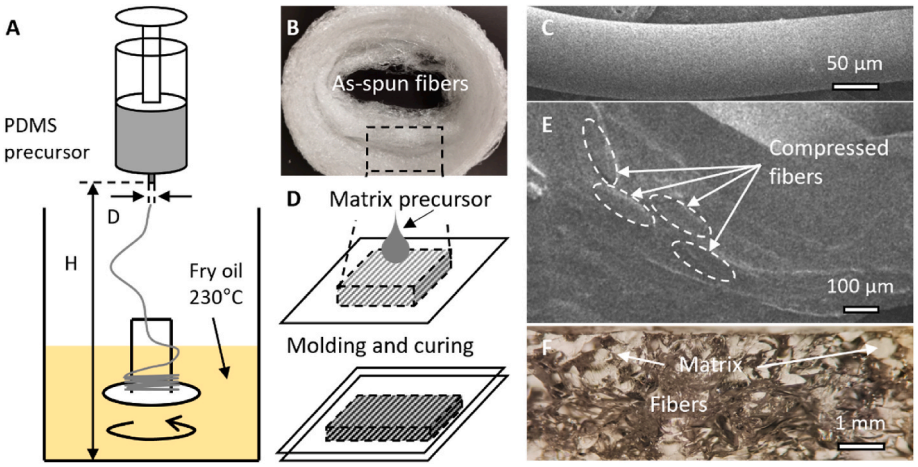

Fig. 4. Fry-spinning and single-phase PDMS composites. (**A**) Schematics of fry-spinning of PDMS microfibers. (**B**) Photos of the fry spun PDMS fiber bundle. (**C**) SEM images of fry spun PDMS microfibers. (**D**) The composites were prepared by soaking microfibers in matrix precursors. (**E**) SEM and (**F**) optical microscopy images of the cross-section of the single-phase PDMS composites.

40% of sample length in grooved PDMS with $a = 0.5$ mm and $w = 1$ mm (Fig. 3C), and more than 25% of sample length in grooved PDMS with $a = 0.5$ mm and $w = 0.5$ mm (Fig. 3D).

These results supported that the fatigue threshold was determined by how much stretch around the crack tip can be distributed along the cracks, or in the simple model here, the ratio of thickness and width a/w. Under repeated cycles of loading, the crack can propagate by just breaking one single polymer chain. However, they formed a triangular front when denting into thick patterns. The sides of the crack front delocalized the stretch of polymer chains around the crack tip. Consequently, the polymer chains around the crack tip did not experience over concentrated stretch and well survived from prolonged loading.

3.2. Fry-spinning

This simple model showed that the stretch on the crack tip can be delocalized by architecture design. This has inspired our single-phase PDMS composites. The composites were made by fibers and matrices of the same PDMS but different crosslinking methods.

We first developed the "fry-spinning" technique to fabricate PDMS fibers with a wide range of diameter. PDMS is a thermosetting polymer that has a long crosslinking time, making fabrication of PDMS fibers extremely challenging. Current methods used coaxial electrospinning to produce polyvinylpyrrolidone fibers with liquid PDMS precursors inside [31]. PDMS is cured inside the polyvinylpyrrolidone which is then dissolved to retrieve PDMS nanofibers. However, these fibers are generally fragile nanofibers [32,33], not suitable for load-bearing application. The "fry-spinning" technique utilizes high temperature to dramatically accelerate the curing of most thermosetting polymers, so that they can form microfibers while spinning. This technique is versatile and could extend to many other thermosetting polymers.

To produce PDMS microfibers, a liquid PDMS precursor was prepared with a base to curing agent ratio of 10:1. The precursor was extruded through syringe needles into a stirring oil bath (230 °C) and cured immediately into microfibers (Fig. 4A). The fibers were collected by a stirring frame and degreased in isopropanol alcohol (Fig. 4B). The fiber diameter is controlled collectively by the viscosity of liquid precursor, inner diameter of syringe needles, D, and height between syringe needles and hot plate, H. For freshly prepared precursor and $H = 200$ mm, the diameter of fibers spun by a 10 ml syringe was between 300 and 500 μm. It was around 100 μm when drawn from an 18-gauge needle (Fig. 4C), and 50 μm from a 24-gauge needle. Fibers were bundled but not rigorously aligned.

Here we chose a fiber diameter of 100 μm to achieve the bridging effect. This is a balance between fiber robustness and flaw sensitivity. On one hand, thick fibers have a larger bending stiffness, resisting bulking during cyclic loading, and are thus beneficial for implementing bridging effects. On the other hand, the fiber diameter must be small compared to the flaw-sensitive length of hydrogels and elastomers, which is usually larger than 100 μm [34]. When the fiber diameter is thicker than the flaw sensitive length, the movement of fibers itself could create new cracks.

3.3. Single-phase stretchable composites

The composites were prepared by soaking microfibers in matrix precursors (Fig. 4D). The precursor infiltrated and infused into fibers under the vacuum, then the infused fiber bundles were pressured to desired volume and shape. The pressure was maintained until the matrix cured.

Three different matrix precursors were used to study how to implement the crack bridging effect in soft composites.

1. The same precursor used for fibers, the base to curing agent ratio was 10:1. The produced composites were denoted as R-R, as both fibers and matrices were cured by radical reaction. The R-R had the same fibers and matrices. It was almost identical to one piece of PDMS and transparent like a homogeneous PDMS.
2. The base to curing agent ratio was 30:1, and the produced composites were denoted as R-RS. Both fibers and matrices were cured by radical reaction, but due to the insufficient curing agent, strong chemical crosslinks formed between fibers and matrices.
3. The base to curing agent ratio was 10:1, but a platinum catalyzer was added. Under the catalysis, matrix polymer chains crosslink quickly via addition reaction. This avoided the most chemical crosslinks between fibers and matrices. Although chemically separated, fibers and matrices were mechanically one material, as fibers screwed into matrices. This chemically separated but mechanically integrated composite was denoted as R–Pt.

Generally, the R–Pt and R-RS followed opposite strategies. R-RS had a strong chemical bonding between fibers and matrices, while R–Pt had almost no chemical bonding but a strong mechanical bonding. The strong mechanical bonding is owing to the architectural confinement of fibers by matrices. SEM images showed that they were completely integrated into one material (Fig. 4E), although architecture inside R–Pt was very complex as shown under light (platinum catalyzer changed the transparency of PDMS, Fig. 4F).

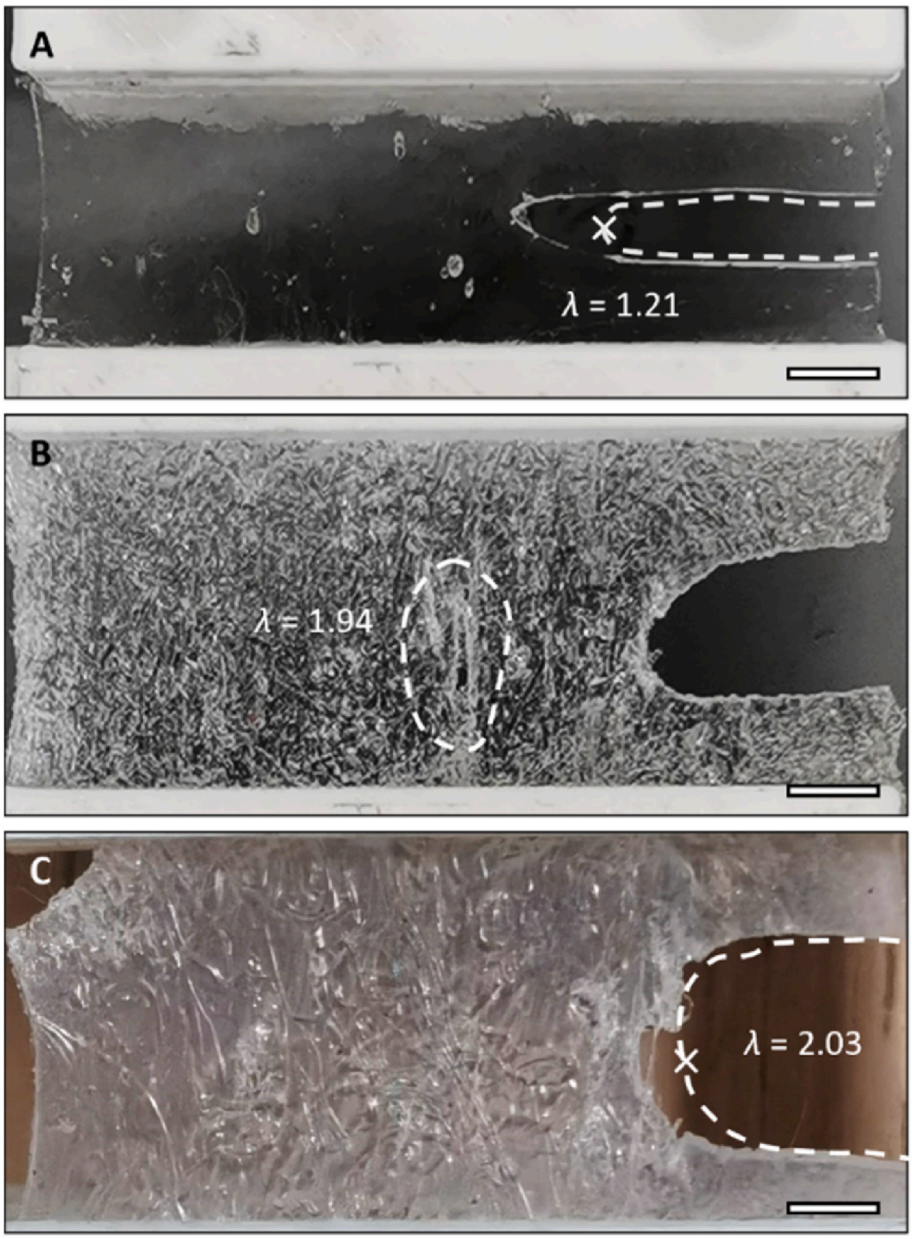

Fig. 5. Fracture toughness measurements for (**A**) thin and wide features, (**B**) thin and small features, (**C**) thick and large features. Scale bar = 5 mm.

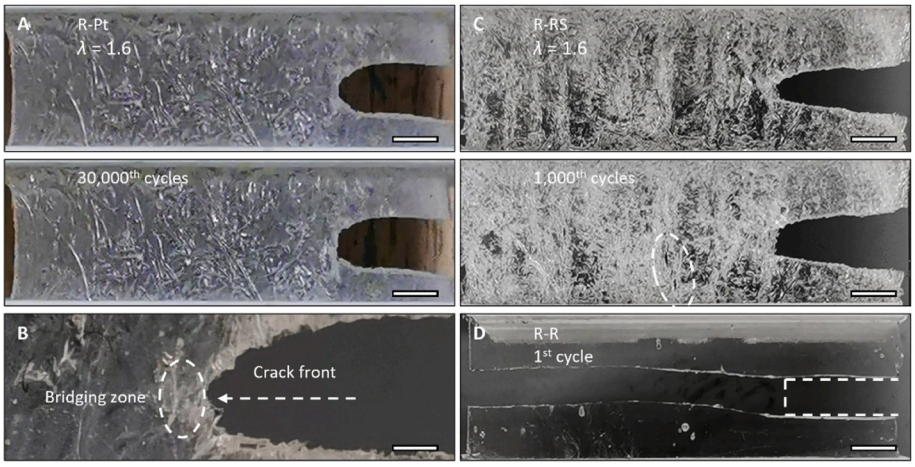

Fig. 6. Crack bridging enhanced fatigue resistance. (**A**) Crack growth in single-phase PDMS composites of radical curing-fibers and platinum curing-matrices. (**B**) Chemically independent fibers formed a bridging zone to compete against the opening trend. (**C**) New cracks (encircled) formed in the composite of radical curing-fibers and much softer radical curing-matrices. This composite design followed the high-energy phase principle. (**D**) Composites of radical curing-fibers and the same radical curing-matrices were as brittle as homogeneous PDMS. Scale bar = 5 mm.

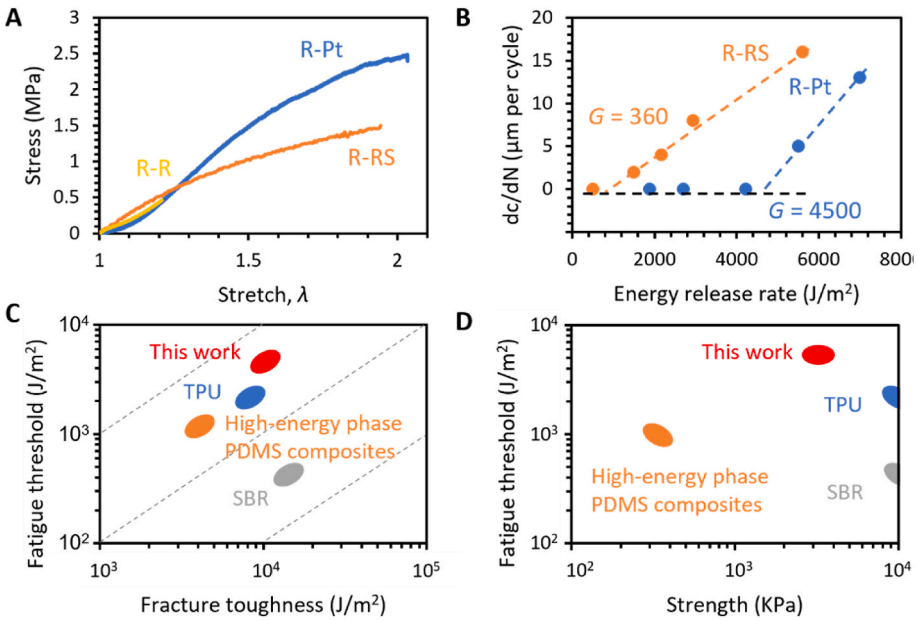

Fig. 7. Fracture toughness, fatigue threshold, and comparisons. (**A**) Stress-stretch curves for toughness measurements. (**B**) Measurements of fatigue thresholds. (**C**) Threshold-toughness chart and (**D**) Threshold-strength chart compare this work with the PDMS-hydrogel composite designed based on the classic principle of high-energy phase [24], and two of the most widely used stretchable materials in industries: TPU (thermoplastic polyurethan) and SBR (styrene-butadiene rubber) [35].

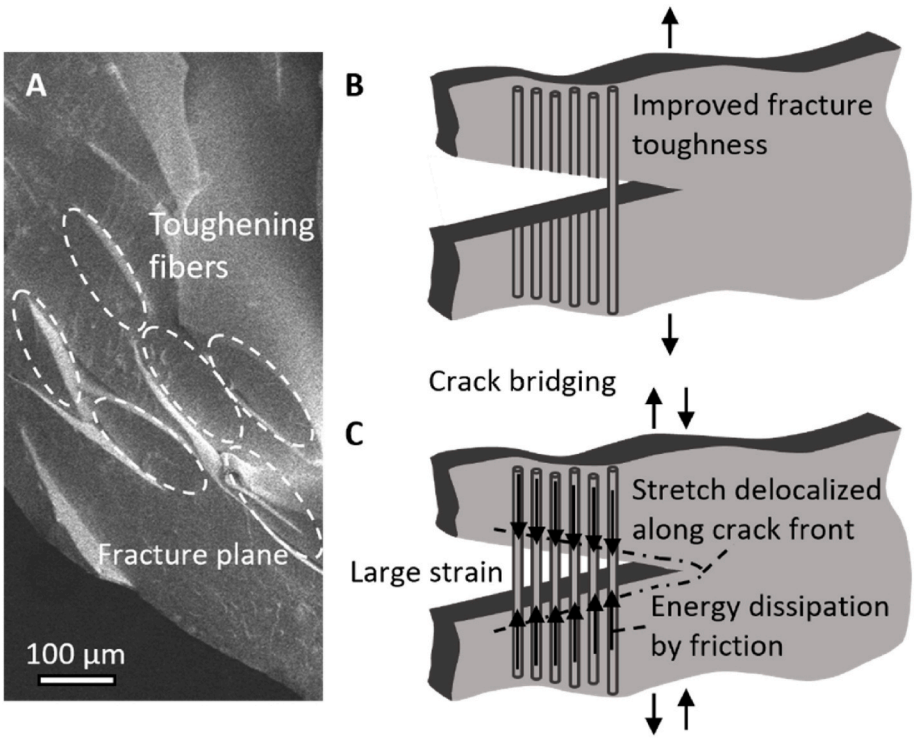

Fig. 8. Proposed mechanisms of crack bridging effect in resisting crack propagation. (**A**) SEM images of the fracture plan of PDMS composites, fibers are independent from matrices. (**B**) Proposed mechanism of the improved fracture toughness in PDMS composites. The crack must fracture whole fibers to propagate. (**C**) Proposed mechanism of the improved fatigue resistance in PDMS composites. The stretch of crack front is delocalized due to energy dissipation by friction over large strains.

3.4. Resisting crack tip by bridging effect

We compared the fracture toughness and fatigue threshold of these three composites. Under one single cycle of stretch, R-R was as brittle as homogeneous PDMS, the crack ran quickly through the entire PDMS (Fig. 5A). By contrast, R-RS and R–Pt fractured only after fibers ruptured. However, their failure modes were different. R-RS broke at the interface between fibers and matrices ahead of crack (Fig. 5B), due to their strong chemical adhesions. On the other hand, in R–Pt, cracks expanded by fracturing fibers in the bridging zone (Fig. 5C).

When loaded repeatedly to $\lambda = 1.6$ for 30,000 cycles, the R–Pt maintained their integrity and prevented crack growth (Fig. 6A). In front of cracks, the composite became less transparent, due to independent movement of fibers against matrices (Fig. 6B). This opaque region was the bridging zone, where the stressed fibers held matrices to compete against the opening trend. Cracks did not propagate unless the bridging

fibers ruptured. In comparison, although R-RS, following the high-energy phase principle, blunted cracks by fibers, new cracks formed at the fiber-matrix interfaces as early as 1000 cycles (Fig. 6C), and fibers started to peel off from matrices. Those new cracks appeared to be independent of the pre-cut cracks and were a result of rigid adhesions between fibers and matrices. The R-R again behaved like a piece of homogeneous material. Fibers in R-R ruptured together with matrices and failed to play any role in resisting cracks (Fig. 6D).

R–Pt had a toughness over 10,000 J/m^2 (Fig. 7A), much larger than the toughness of R-R and R-RS. Low toughness of R-R was mainly because of its small critical stretch, while the toughness of R-RS was limited by its low Young's modulus. R–Pt also had a fatigue threshold of around 4500 J/m^2 (Fig. 7B), one order of magnitude higher than the fatigue threshold of R-RS. The fatigue threshold of R-RS was largely restricted by the formation of new cracks.

The results showed that only fibers in R–Pt invoked the crack bridging effect. Therefore, to implement crack bridging, fibers and matrices should be chemically disconnected but mechanically integrated. When subjected to large stretches, the strong friction forces between fibers and matrices due to architecture confinement can well dissipate energy of the crack front. Under a single cycle of loading, fibers were independent from cracks (Fig. 8A). To propagate, the crack must fracture the whole fibers (Fig. 8B). The fiber-matrix friction and rupture of fibers dramatically dissipate energy around the crack. Under the repeated cycles of loading, cracks were allowed to dent into matrices between fibers. The longer the crack penetrates, the more energy is dissipated by the friction forces over large stretches. The stretch of single polymer chains was thus delocalized along around the crack tip (Fig. 8C).

Crack bridging has been widely adopted in many biological fiber materials [36], and fiber reinforced composites [37]. Like them, the success of our single-phase PDMS relies on the forces between fibers and matrices to "close" the opening of crack. However, unlike the biological fibers and composites, the fiber-matrix or fiber-fiber connections in our single-phase PDMS are much weaker. This is because the crack stretchable matrices can easily propagate into stretchable fibers via chemical crosslinks between polymer chains [12]. To avoid the possible crack growth from matrices into fibers, we use different crosslinking mechanisms for fibers and matrices to chemically separate them. In the meantime, the strong physical friction between fibers and matrices provides the "closing" force needed to delocalize stretch. The use of friction over chemical bonding is largely because the stretchable matrices and fibers undergo a large strain and strain rate. For example, the cyclic strain in our experiments was above 50% and the strain rate was as large as 100%/s. The strong friction force over such large strains can effectively dissipate energy of the crack front. The chemically weak bonded fiber-matrix interaction has also been adopted by ceramic composites [38], and successfully applied in commercial aircraft engines [39]. Both ceramic composites and our stretchable composites rely on the separation of fibers and matrices to isolate the crack. However, the ceramic composites do not have perfect geometric match to provide strong friction, due to the porosity formation, and they do not experience large strain to dissipate energy.

3.5. Compare to high-energy phase principle and industrial materials

When compared to reported PDMS composites designed based on the classic principle of high-energy phase, the single-phase PDMS composites had both much higher toughness and threshold (Fig. 7C). More importantly, they did not compromise their strength and modulus (Fig. 7D). A high strength is required for load-bearing and general-purpose applications, as shown by two of the most widely used stretchable materials in industries: thermoplastic polyurethane (TPU), an industrial grade fatigue resistant elastomers [35], and styrene-butadiene rubber (SBR), the highest volume synthetic rubber in production [40]. When compared to TPU and SBR, the single-phase PDMS composites had a much higher fatigue threshold, 1.73 times of the threshold of TPU and one order of magnitude higher than the threshold of SBR.

4. Conclusion

In this paper, we first demonstrated that structural design could utilize crack bridging to improve the fatigue resistance of micro-patterned PDMS. Next, we applied this principle by creating structurally integrated but molecularly separated single-phase PDMS composites. The resultant composites had a fracture toughness of 10,000 J/m^2, and fatigue threshold of 4500 J/m^2. In comparison, PDMS-hydrogel composites designed based on classic high-energy phase principle had a threshold of 1250 J/m^2, and TPU, the widely used fatigue resistant elastomers in many industries, had a threshold of 2600 J/m^2. This work proves the feasibility of utilizing crack bridging for fatigue resistance and provides an alternative design direction for stretchable materials whose polymer chains cannot form high-energy phases.

CRediT author statement

Mingkun Wang: conceptualization, methodology, project administration, writing – original draft preparation, writing – reviewing and editing. Dani Liu: investigation, formal analysis, visualization, writing – original draft preparation, writing – reviewing and editing. Shuofei Sun: investigation, formal analysis. Gening Dong: investigation, formal analysis. Feifei Long: investigation, formal analysis.

Declaration of competing interest

The authors declare that they have no known competing financial interests or personal relationships that could have appeared to influence the work reported in this paper.

Data availability

Data will be made available on request.

Acknowledgements

This work was supported by AHA grant 821615 and relied on equipment supported by NSF award DMR-1719875.

References

[1] Rus D, Tolley MT. Design, fabrication and control of soft robots. Nature 2015;521(7553):467–75.
[2] Liu B, Feng J, Yu K, Li J, Hu Q, Lin Z, et al. Three-dimensional auxetic structure design methods based on bulking-induced deformation and the application in soft crawling robot. Compos B Eng 2022;244:110146.
[3] Zhang X, Tian M, Raza T, Zhao H, Wang J, Du X, et al. Soft robotic reinforced by carbon fiber skeleton with large deformation and enhanced blocking forces. Compos B Eng 2021;223:109099.
[4] Wang Q, Wu Z, Huang J, Du Z, Yue Y, Chen D, et al. Integration of sensing and shape-deforming capabilities for a bioinspired soft robot. Compos B Eng 2021;223:109116.
[5] Someya T, Bao Z, Malliaras GG. The rise of plastic bioelectronics. Nature 2016;540(7633):379–85.
[6] Barshutina MN, Kirichenko SO, Wodolajsky VA, Lopachev AV, Barshutin SN, Gorsky OV, et al. PDMS-CNT composite for soft bioelectronic neuronal implants. Compos B Eng 2022;247:110286.
[7] Zhou Z, He Z, Yin S, Xie X, Yuan W. Adhesive, stretchable and antibacterial hydrogel with external/self-power for flexible sensitive sensor used as human motion detection. Compos B Eng 2021;220:108984.
[8] Cui H, Jiang W, Wang C, Ji X, Liu Y, Yang G, et al. Lignin nanofiller-reinforced composites hydrogels with long-lasting adhesiveness, toughness, excellent self-healing, conducting, ultraviolet-blocking and antibacterial properties. Compos B Eng 2021;225:109316.
[9] Wang M, Sun S, Dong G, Long F, Butcher JT. Soft, strong, tough, and durable protein-based fiber hydrogels. Proc Natl Acad Sci USA 2023;120(8):e2213030120.
[10] Yang X, Li S, Ren Y, Qiang L, Liu Y, Wang J, et al. 3D printed hydrogel for articular cartilage regeneration. Compos B Eng 2022;237:109863.

[11] Zhu T, Gu H, Ma W, Zhang Q, Du J, Chen S, et al. A fabric reinforced small diameter tubular graft for rabbits' carotid artery defect. Compos B Eng 2021;225:109274.
[12] Bai R, Yang J, Suo Z. Fatigue of hydrogels. Eur J Mech Solid 2019;74:337–70.
[13] Bai R, Yang J, Morelle XP, Yang C, Suo Z. Fatigue fracture of self-recovery hydrogels. ACS Macro Lett 2018;7(3):312–7.
[14] Zhang W, Liu X, Wang J, Tang J, Hu J, Lu T, et al. Fatigue of double-network hydrogels. Eng Fract Mech 2018;187:74–93.
[15] Bai R, Yang Q, Tang J, Morelle XP, Vlassak J, Suo Z. Fatigue fracture of tough hydrogels. Extr Mech Lett 2017;15:91–6.
[16] Lin S, Liu X, Liu J, Yuk H, Loh H-C, Parada GA, et al. Anti-fatigue-fracture hydrogels. Sci Adv 2019;5(1):eaau8528.
[17] Liang X, Chen G, Lin S, Zhang J, Wang L, Zhang P, et al. Bioinspired 2D isotropically fatigue-resistant hydrogels. Adv Mater 2022;34(8):2107106.
[18] Liang X, Chen G, Lin S, Zhang J, Wang L, Zhang P, et al. Anisotropically fatigue-resistant hydrogels. Adv Mater 2021;33(30):2102011.
[19] Ni J, Lin S, Qin Z, Veysset D, Liu X, Sun Y, et al. Strong fatigue-resistant nanofibrous hydrogels inspired by lobster underbelly. Matter 2021;4(6):1919–34.
[20] Lin S, Liu J, Liu X, Zhao X. Muscle-like fatigue-resistant hydrogels by mechanical training. Proc Natl Acad Sci USA 2019;116(21):10244–9.
[21] Li X, Cui K, Sun TL, Meng L, Yu C, Li L, et al. Mesoscale bicontinuous networks in self-healing hydrogels delay fatigue fracture. Proc Natl Acad Sci USA 2020;117(14):7606–12.
[22] Bai R, Yang J, Morelle XP, Suo Z. Flaw-insensitive hydrogels under static and cyclic loads. Macromol Rapid Commun 2019;40(8):1800883.
[23] Wang Z, Xiang C, Yao X, Floch PL, Mendez J, Suo Z. Stretchable materials of high toughness and low hysteresis. Proc Natl Acad Sci USA 2019;116(13):5967–72.
[24] Xiang C, Wang Z, Yang C, Yao X, Wang Y, Suo Z. Stretchable and fatigue-resistant materials. Mater Today 2020;34:7–16.
[25] Zhao X, Chen X, Yuk H, Lin S, Liu X, Parada G. Soft materials by design: unconventional polymer networks give extreme properties. Chem Rev 2021;121(8):4309–72.
[26] Hua M, Wu S, Ma Y, Zhao Y, Chen Z, Frenkel I, et al. Strong tough hydrogels via the synergy of freeze-casting and salting out. Nature 2021;590(7847):594–9.
[27] He Q, Huang Y, Wang S. Hofmeister effect-assisted one step fabrication of ductile and strong gelatin hydrogels. Adv Funct Mater 2018;28(5):1705069.
[28] Ritchie RO. The conflicts between strength and toughness. Nat Mater 2011;10(11):817–22.
[29] Bouville F, Maire E, Meille S, Van de Moortèle B, Stevenson AJ, Deville S. Strong, tough and stiff bioinspired ceramics from brittle constituents. Nat Mater 2014;13(5):508–14.
[30] Chen X, Cheng G, Yang J, Hu J, Liao C, Zhang X, et al. Effects of interfacial residual stress on mechanical behavior of SiCf/SiC composites. J Adv Ceram 2022;11(1):94–104.
[31] Niu H, Wang H, Zhou H, Lin T. Ultrafine PDMS fibers: preparation from in situ curing-electrospinning and mechanical characterization. RSC Adv 2014;4(23):11782–7.
[32] Xue J, Wu T, Dai Y, Xia Y. Electrospinning and electrospun nanofibers: methods, materials, and applications. Chem Rev 2019;119(8):5298–415.
[33] Kong B, Liu R, Guo J, Lu L, Zhou Q, Zhao Y. Tailoring micro/nano-fibers for biomedical applications. Bioact Mater 2023;19:328–47.
[34] Chen C, Wang Z, Suo Z. Flaw sensitivity of highly stretchable materials. Extr Mech Lett 2017;10:50–7.
[35] Scetta G, Selles N, Heuillet P, Ciccotti M, Creton C. Cyclic fatigue failure of TPU using a crack propagation approach. Polym Test 2021;97:107140.
[36] Meng Q, Gao Y, Shi X, Feng X-Q. Three-dimensional crack bridging model of biological materials with twisted Bouligand structures. J Mech Phys Solid 2022;159:104729.
[37] Meng Q, Li B, Li T, Feng X-Q. A multiscale crack-bridging model of cellulose nanopaper. J Mech Phys Solid 2017;103:22–39.
[38] Wang P, Liu F, Wang H, Li H, Gou Y. A review of third generation SiC fibers and SiCf/SiC composites. J Mater Sci Technol 2019;35(12):2743–50.
[39] Steibel J. Ceramic matrix composites taking flight at GE Aviation. Am Ceram Soc Bull 2019;98(3):30–3.
[40] Zhong J, Luo Z, Hao Z, Guo Y, Zhou Z, Li P, et al. Enhancing fatigue properties of styrene butadiene rubber composites by improving interface adhesion between coated aramid fibers and matrix. Compos B Eng 2019;172:485–95.